EFFECTS OF THE MPM DISCRETISATIONS ON SOIL-STRUCTURE PROBLEMS

S. FATEMIZADEH[1], F. HAMAD[2] AND C. MOORMANN[3]

[1]University of Stuttgart
Institute of Geotechnical Engineering (IGS)
Pfaffenwaldring 35, 70569 Stuttgart, Germany
e-mail: farzad.fatemizadeh@igs.uni-stuttgart.de, URL: http://www.uni-stuttgart.de/igs/

[2] University of Stuttgart
Institute of Geotechnical Engineering (IGS)
Pfaffenwaldring 35, 70569 Stuttgart, Germany
e-mail: fursan.hamad@igs.uni-stuttgart.de, URL: http://www.uni-stuttgart.de/igs/

[3] University of Stuttgart
Institute of Geotechnical Engineering (IGS)
Pfaffenwaldring 35, 70569 Stuttgart, Germany
e-mail: christian.moormann@igs.uni-stuttgart.de, URL: http://www.uni-stuttgart.de/igs/

Key words: Large deformation, MPM discretisations, Strip footing.

Abstract. Material point method (MPM) is a mesh based particle method which is suitable to simulate applications with large deformations. MPM adopts two discretisations, one is the space discretisation where the equation of motion is solved, and the other is the material discretisation where the continuum is replaced by material points or particles. Particles are allowed to move through the background computational mesh, which allows MPM to simulate large displacements and deformations of the material [9].

The effect of the spatial discretisation on the simulation results have been studied by others e.g. [1] considering a specific application like bending of a cantilevered beam. More generally, the sensitivity of the MPM solution to the two discretisations specially when dealing with bench mark problems in the field of geotechnical engineering has not been considered so far, although the method is applied widely in this area e.g. [2,13].

In this paper, the well-known problem in the field of geotechnical engineering is analyzed using MPM. In the case of available reference solutions the results are then evaluated. The effects of the two MPM discretisations on the quality of the final results have been investigated where some concluding remarks are presented.

1 INTRODUCTION

Since the formulation of Finite Element Method (FEM) is introduced, it has been used in different fields of engineering especially geotechnical engineering. This method has been shown its capabilities to simulate different phenomena. Considering applications include large deformations or displacements, FEM is not able to predict the behaviour of the continuum and suffers from the mesh distortion. During the simulation the mesh becomes so distorted which

causes numerical difficulties. In the field of geotechnical engineering, large deformations of the soil become evident in many applications e.g. sliding of slopes, failure of strip footing, pile driving, etc. which require other numerical schemes for simulating and studying them.

Available numerical methods for simulating large deformations can be categorized into three major groups. In the first group, the methods use the advantages of the both Lagrangian and Eulerian descriptions of motion while avoiding their drawbacks. The Arbitrary Lagrangian Eulerian (ALE) method [3] and the Coupled Eulerian Lagrangian (CEL) method [4] are categorized in this group. Second group includes the mesh free methods like the Element Free Galerkin (EFG) method [5] and the Smooth Particle Hydrodynamic (SPH) method [6]. The last group contains the mesh based particle methods. The Particle in Cell (PIC) method [7], Fluid Implicit Particle (FLIP) method [8] and the Material Point Method (MPM) [9,10] are recognized in this group.

MPM discretises the continuum using the material points or particles and discretises the space using an Eulerian background fixed mesh on which the equations of motion are solved. This mesh should cover the whole space where the material may go during the simulation process. Material points are the integration points which can move during the simulation. Using this property, MPM is able to analyze large deformations where particles carry all the permanent information (e.g. stresses, strain, etc.) during the simulation process and no permanent data are stored on the mesh.

Solution procedure of MPM for one time step consists of three phases. First is the initialization phase where all the data are mapped from particles to the nodes of the background mesh. Then is the Lagrangian phase in which the equations of motion are solved on the mesh. At the end is the convective phase in which information are mapped back from the mesh to the material points and updates the data of the particles. The background mesh goes back to its original position (as shown in Figure 1).

Sulsky et al. [9] applied the PIC method from fluid to solid mechanics and called it the material point method [10]. Bardenhagen et al. [11] introduced a frictional contact algorithm to the method based on the Coulomb friction law. Bardenhagen and Kober [12] presented the Generalized Interpolation Material Point Method (GIMP) to avoid the grid crossing error presented in the framework of original MPM. As MPM showed its capability to simulate the dynamics of large deformation, the method is adopted to investigate many applications in the field of geotechnical engineering [2,13].

The two discretisations in MPM (space discretization and the material discretization) play important role in the quality of the final results. The effects of the interpolation order of discretisation for a cantilevered beam is studied by Anderson and Anderson [1]. They showed that the best results for the small strain problems can be obtained using the quadratic shape functions whereas the cubic splines show better results for the large strain cases. The size of the mesh as well as the number of particles per element can also affect the simulation results.

In this paper the effects of the two discretisations on the strip footing problem are studied. For the sake of completeness, a short description on the governing equations of MPM are discussed then the enhanced volumetric strain method to overcome the volumetric locking that happens in low order elements are briefly explained [2,15]. Next the strip footing problem is analyzed using different combinations of the meshes. At the end of this paper, some conclusion remarks are presented.

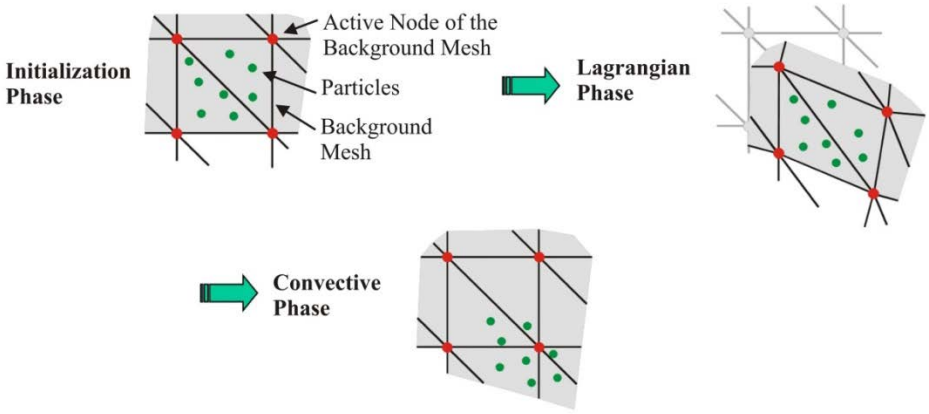

Figure 1: MPM discretisations and the solution procedure for one time step

2 GOVERNING EQUATIONS

The starting point is the Cauchy form of the conservation of linear momentum

$$\rho\ddot{\boldsymbol{u}} = \nabla \cdot \boldsymbol{\sigma} + \rho \boldsymbol{g} \quad and \quad \boldsymbol{t} = \boldsymbol{\sigma} \cdot \boldsymbol{n} \tag{1}$$

where ρ is the material density, **u** is the displacement, a superposed dot declares differentiation with respect to time, **σ** is the Cauchy stress tensor and **g** is the gravitational acceleration vector. The surface traction acting on the external boundary is denoted by **t** and **n** is the outward unit normal of the boundary. Applying the virtual work principle on a domain of volume V surrounded by boundary S yields

$$\int_V w\boldsymbol{u}^T \rho \ddot{\boldsymbol{u}} dV = -\int_V w\boldsymbol{\varepsilon}^T \boldsymbol{\sigma} dV + \int_V w\boldsymbol{u}^T \rho \boldsymbol{g} dV + \int_S w\boldsymbol{u}^T \boldsymbol{t} dS \tag{2}$$

where w denotes a virtual quantity, **ε** is the strain tensor and the superscript T specifies the transpose.

For space discretization, the displacement field **u** is approximated in terms of the shape functions **N** and nodal displacements **a**. Then displacement and strain can be written as

$$\boldsymbol{u} = \boldsymbol{N}\boldsymbol{a} \tag{3}$$

$$\boldsymbol{\varepsilon} = \boldsymbol{B}\boldsymbol{a} \qquad \boldsymbol{B} = \boldsymbol{L}\boldsymbol{N} \tag{4}$$

where **B** is the strain displacement matrix, **L** is a linear differential operator. Substituting Eq. (3) and Eq. (4) into Eq. (2) gives [9,10]

$$\boldsymbol{M}\ddot{\boldsymbol{a}} = \boldsymbol{F}^{ext} - \boldsymbol{F}^{int} \tag{5}$$

in which

$$\boldsymbol{M} = \int_V \rho \boldsymbol{N}^T \boldsymbol{N} dV \tag{6}$$

$$\boldsymbol{F}^{ext} = \int_V \rho \boldsymbol{N}^T \boldsymbol{g} dV + \int_S \boldsymbol{N}^T \boldsymbol{t} dS \tag{7}$$

$$\boldsymbol{F}^{int} = \int_V \boldsymbol{B}^T \boldsymbol{\sigma} dV \,. \tag{8}$$

Eq. (5) is identical in the context of FEM and MPM.

To increase the computational efficiency, the consistent mass matrix Eq. (6) is lumped. The drawback of using a lumped mass matrix is a slight dissipation in the kinetic energy [14].

The particle discretization is achieved via approximating the continuous density field using the Dirac delta function (δ), such that

$$\rho(\boldsymbol{x}) = \sum_{P=1}^{n_p} m_p \delta(\boldsymbol{x} - \boldsymbol{x}^p) \tag{9}$$

where $\boldsymbol{x}$ is an arbitrary position vector, $\boldsymbol{x}^p$ is the position vector at particle p. By considering this approximation into account, Eq. (6), Eq. (7) and Eq. (8) can be rewritten as

$$\begin{gathered} \boldsymbol{M}_L = \begin{bmatrix} m_1 & \cdots & 0 \\ \vdots & \ddots & \vdots \\ 0 & \cdots & m_n \end{bmatrix} \\ m_i = \sum_{p=1}^{n_p} m_p N_i^p \end{gathered} \tag{10}$$

$$\boldsymbol{F}^{int} = \sum_{P=1}^{n_p} \boldsymbol{B}_P^T \boldsymbol{\sigma}_P V_P \tag{11}$$

$$\boldsymbol{F}^{ext} = \sum_{P=1}^{n_p} N_i^P m_P \boldsymbol{g} + \sum_{P=1}^{n_p} N_i^P \boldsymbol{t}_P \tag{12}$$

where $\mathrm{V_P}$ is the volume associated to particle P and $\mathbf{t_P}$ is the force vector from the surface traction mapped to the boundary particle P.

Most of the MPM applications are based on the explicit time integration scheme. This method is conditionally stable and the time step size should be smaller than the critical time (Δt_{cr}) step value dictated by the CFL condition

$$\Delta t_{cr} = {}^{h_{min}}/_{c_d} \tag{13}$$

where $\mathrm{h_{min}}$ is the minimum representative distance in an element and $\mathrm{c_d}$ is the compression wave speed.

Explicit time integration of discretised momentum equation is performed via applying Euler forward integration scheme such that

$$\ddot{\boldsymbol{a}}^t = [\boldsymbol{M}_L^t]^{-1} \boldsymbol{F}^t \quad , \qquad \dot{\boldsymbol{a}}_p{}^{t+\Delta t} = \dot{\boldsymbol{a}}_p{}^t + \Delta t \boldsymbol{N}_p \ddot{\boldsymbol{a}}^t \tag{14}$$

where $\Delta\mathrm{t}$ is the time increment, $\dot{\boldsymbol{a}}_p{}^{t+\Delta t}$ and $\dot{\boldsymbol{a}}_p{}^t$ are the particle velocities at time t and $\mathrm{t} + \Delta\mathrm{t}$ respectively and $\ddot{\mathbf{a}}^{\mathrm{t}}$ is the nodal accelerations at time t.

The nodal velocities $\dot{\mathbf{a}}^{\mathrm{t}+\Delta\mathrm{t}}$ at time $\mathrm{t} + \Delta\mathrm{t}$ are then calculated from the updated particles velocities, solving the following equation [9]

$$\boldsymbol{M}_L^t \dot{\boldsymbol{a}}^{t+\Delta t} \approx \sum_{p=1}^{n_p} m_p \boldsymbol{N}_p^T \, \dot{\boldsymbol{a}}_p{}^{t+\Delta t} \tag{15}$$

Vector of nodal displacements is calculated using Euler backward integration method. Then the position of particles $(\boldsymbol{x}_p)$ are updated

$$\begin{aligned} \Delta \boldsymbol{a}^{t+\Delta t} &= \Delta t \dot{\boldsymbol{a}}^{t+\Delta t} \\ \boldsymbol{x}_P^{t+\Delta t} &= \boldsymbol{x}_P^t + \boldsymbol{N}_P \Delta \boldsymbol{a}^{t+\Delta t} \end{aligned} \tag{16}$$

3 ENHANCED VOLUMETRIC STRAIN METHOD

In order to overcome the locking phenomena appears in low order elements being used here, the method suggested by Detournay & Dzik [15] and applied in MPM by Jassim et al. [2] is adopted. This method is based on the nodal volumetric strain averaging. First the strain is decomposed into the volumetric and deviatoric parts, then nodal volumetric strains are computed based on the average volumetric strain of the elements

$$\bar{\dot{\varepsilon}}_{vi} = \frac{\sum_{e=1}^{n_{elem}} \dot{\varepsilon}_{ve} \Omega_e}{\sum_{e=1}^{n_{elem}} \Omega_e} \tag{17}$$

where $\bar{\dot{\varepsilon}}_{vi}$ is the volumetric strain rate on node i, $\dot{\varepsilon}_{ve}$ is the volumetric strain rate of the element e, Ω_e is the volume of e and n_{elem} is the number of elements attached to node i. The smooth volumetric strain of the element is the average of the nodal values obtained from equation (17) in the form

$$\bar{\dot{\varepsilon}}_{ve} = \frac{1}{n_{en}} \sum_{i=1}^{n_{en}} \bar{\dot{\varepsilon}}_{vi} \tag{18}$$

where n_{en} is the number of nodes in an element and $\bar{\dot{\varepsilon}}_{ve}$ is the enhanced volumetric strain of element e. Then the final strain rate tensor of an element is defined as

$$\bar{\dot{\varepsilon}}_{ij} = \dot{\varepsilon}_{ij} - \frac{1}{3}(\dot{\varepsilon}_v - \bar{\dot{\varepsilon}}_v)\delta_{ij} \tag{19}$$

where δ_{ij} is the Kronecker delta. In MPM, equation (19) is applied for all individual material points.

4 NUMERICAL EXAMPLE

In this section the problem of a vertically loaded strip footing for undrained conditions [2] is solved here by developing a 2D MPM programm. The geometry, mesh and boundary conditions are shown in Figure 2. Due to the symmetry only one half of the space is simulated. The analytical solution for this problem is given by Hill [16]

$$q/c = \pi + 2 \tag{20}$$

in which q is the footing pressure and c is the cohesion of the soil.

The soil is assumed to behave according to the Tresca material model with the elastic modulus $\mathrm{E} = 200\ \mathrm{MN/m^2}$, Poisson ratio $\nu = 0.495$, density $\rho = 1800\ \mathrm{kg/m^3}$ and

$c = 100\ \mathrm{kN/m^2}$. The footing pressure is increased gradually in stepwise with an increment of $2\ kN/m^2$.

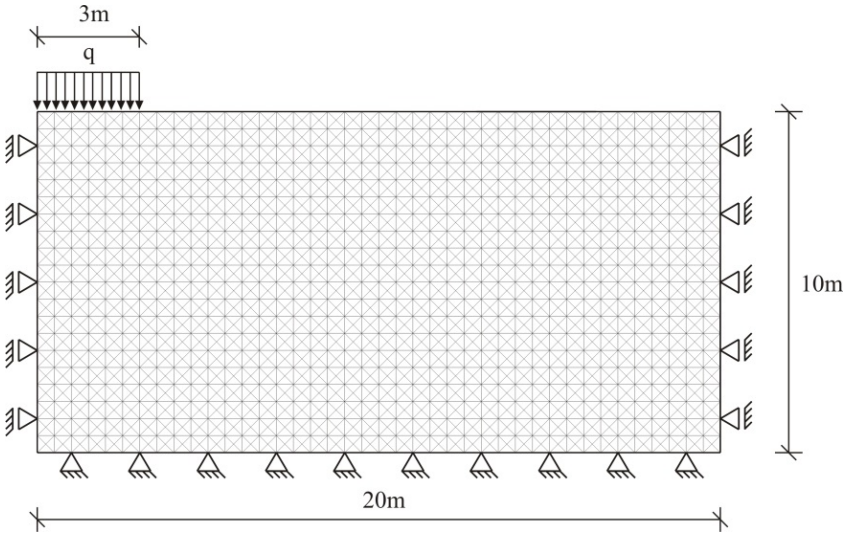

Figure 2: Geometry and boundary conditions of the strip footing problem

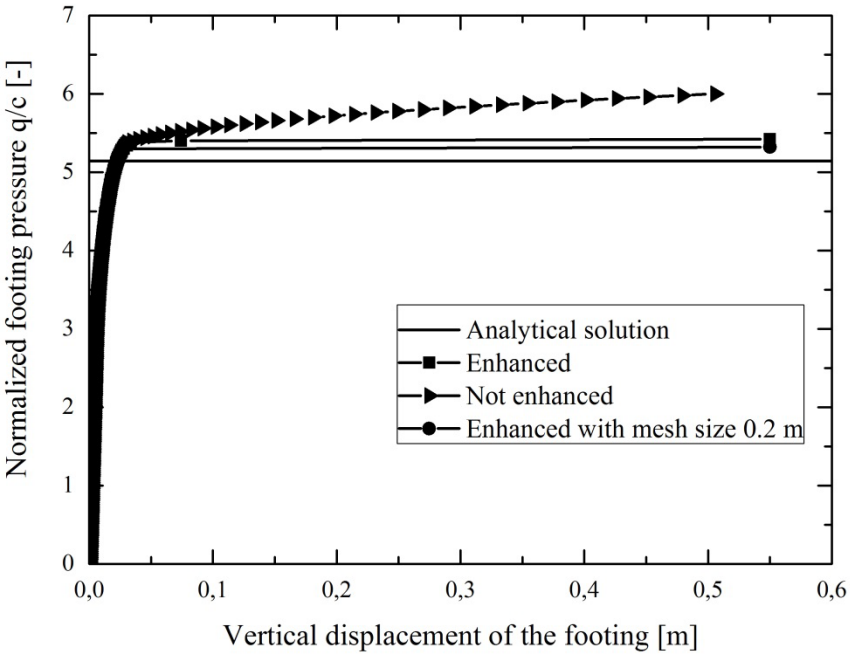

Figure 3: load displacement curve of the strip footing problem

4.1 Effectivity of the enhanced volumetric strain method

To show the effectivity of the enhanced volumetric strain method to mitigate the volumetric locking, the strip footing problem is solved using one particle per element. Small strain deformation is assumed, so the positions of the particles are not updated during the simulation. This problem is solved to evaluate the effect of enhanced volumetric strain

method. Equilibrium conditions are checked in each loading step and after fulfilling the equilibrium conditions the load is increased. The results are shown in Figure 3 together with the analytical solution. From this figure, it can be seen that the enhanced volumetric strain method is able to relax the elements from locking and the curve is nearer to the analytical solution. The gap between the enhanced solution and the analytical solution is attributed to the mesh refinement. By using finer mesh this gap becomes smaller. The same problem is solved using a finer mesh with cell size 0.2 m instead 0.5 m. The results are shown in Figure 3. It is obvious that the finer mesh reduces the distance between the analytical solution and the numerical one.

The effect of applying the load on particles (as performed previously) or on the nodes, furthermore, the effect of updating the location of the particles is analyzed using the mesh of cell size 0.5 m as shown in Figure 4. Applying the load on particles or as in classical FEM on nodes does not affect the results here as we do not updated the locations of the particles, but by updating the particle locations this effect can be seen and the curve deviates from the classical FEM and becomes more separated from the analytical solution.

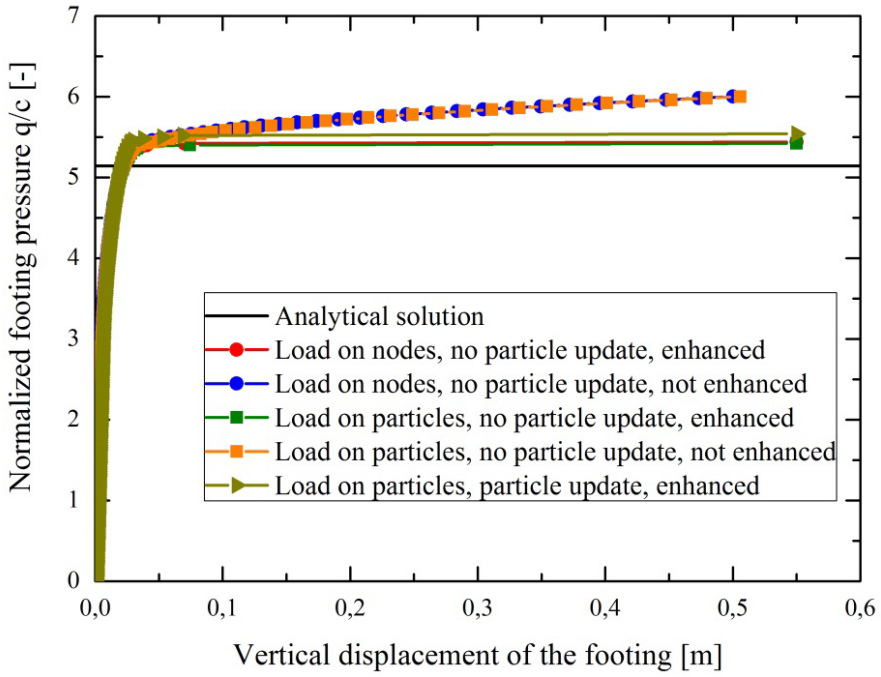

Figure 4: load displacement curve to investigate the effect of applying lods on nodes or particles and updating particle positions

4.2 The effect of the element size

The regular discretization, shown in Figure 2, with 0.5 m cell size has been compared to coarser mesh (1 m) and an unstructured mesh, see Figure 5. Four particles are placed initially inside each element. After applying the self-weight of the soil, the pressure of the footing is increased in stepwise with a value of $2\ \mathrm{kN/m^2}$. After fulfilling the equilibrium conditions, [2], the loading procedure is continued.

Figure 6 shows the vertical displacement of a particle located immediately below the

footing on the left. In this figure the results from the three meshes together with the analytical solution are shown. Results of the cell size 0.5 m and the unstructured mesh are closer to the analytical solution than the coarse mesh. Figure 7 shows the total displacement of the particles using the mesh shown in Figure 2. Figure 8 takes a closer look at the particles displacement below the footing and shows their total displacement. As can be seen from this figure the particles under the footing start to travel to the other elements. As mentioned before, using this property MPM can simulate large deformations, but at the same time the grid crossing error appears which affect the final results.

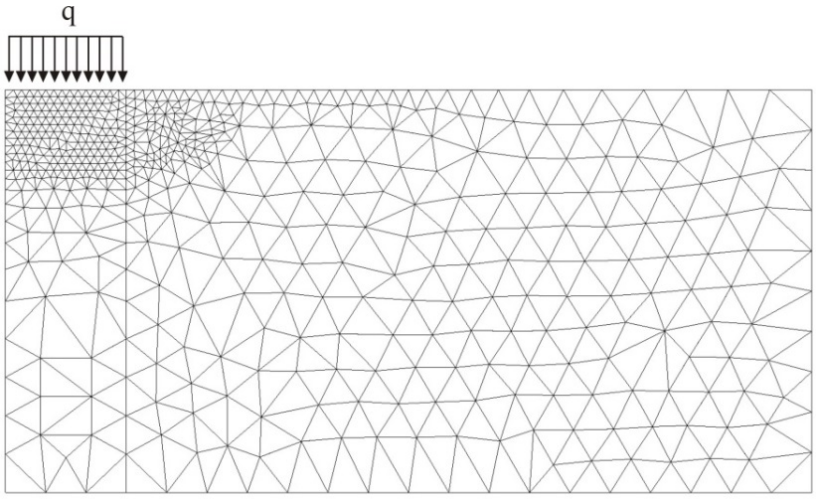

Figure 5: three-noded unstructured mesh

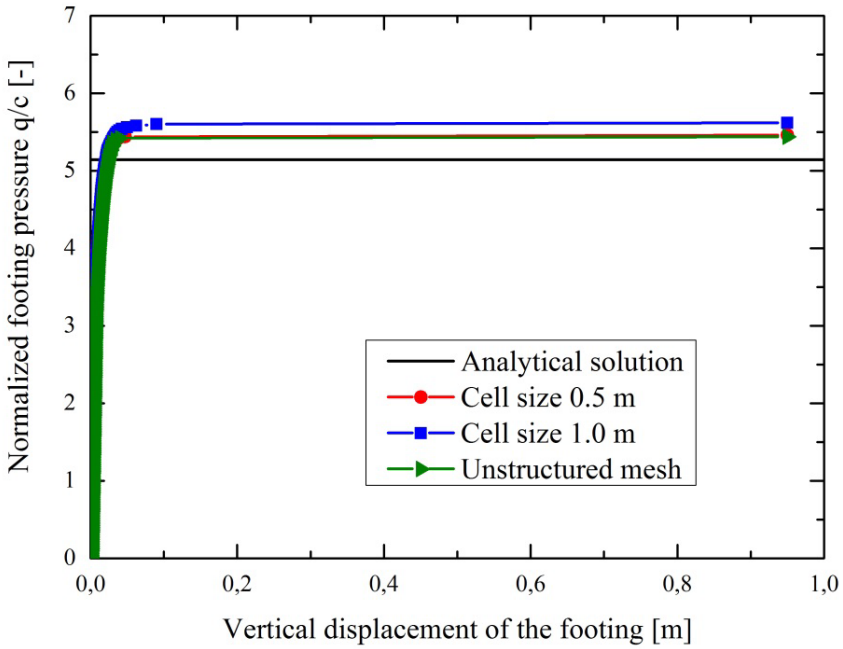

Figure 6: load displacement curve for the three different meshes

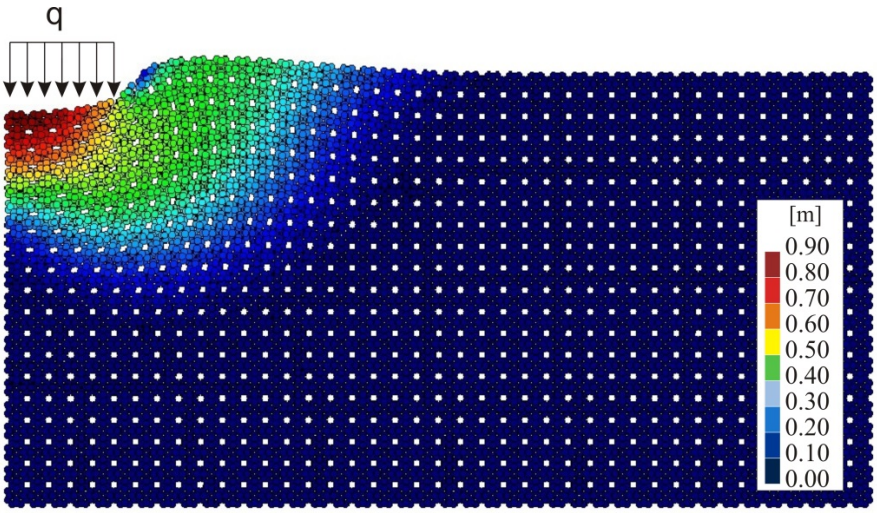

Figure 7: total displacement of the particles using 0.5 m mesh size

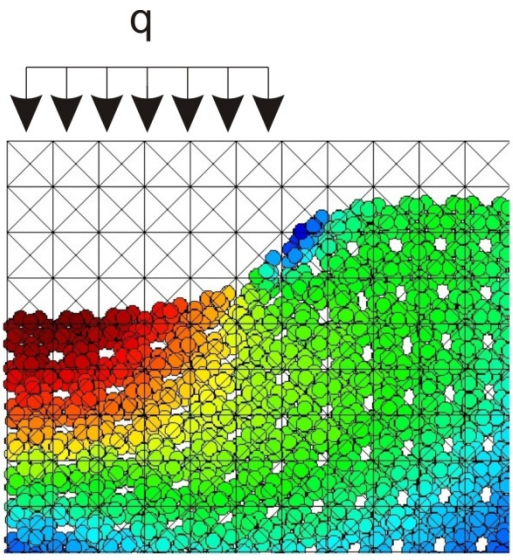

Figure 8: total displacement of the particles using 0.5 m mesh size

4.3 The effect of the number of particles

In this part of the paper, the effect of the initial number of particles per element on the final results of the footing problem is analyzed. A mesh with the cell size of 1.0 m is used with one, four and ten particles per element. The simulations are performed by applying the traction on the boundary particles and allowing the particles to follow the deformation. Figure 9 shows the vertical displacement of a particle located immediately below the footing on the left. As can be seen from Figure 9, no difference can be noticed between the ultimate bearing capacities. Figure 10 but focuses on the displacements between zero and 15 cm of Figure 9. For the same load, the model with initially 10 particles per element shows the smallest deformation. Next is the model with initially four particles per element and then the one with initially one particle per element. It can be concluded that the model with initially ten particles

per element shows more accurate results for the intermediate loading (before failure) than the two other models and the one with initially four particles per element is more accurate than the model with initially one particle per element.

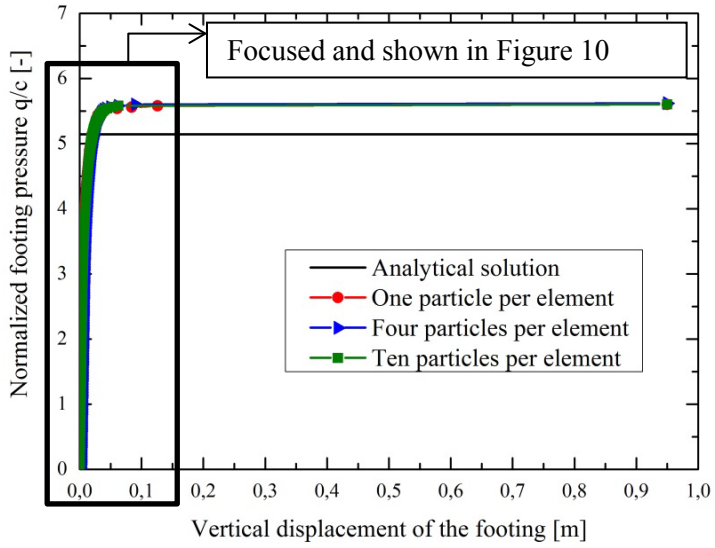

Figure 9: load displacement curve for the three different meshes

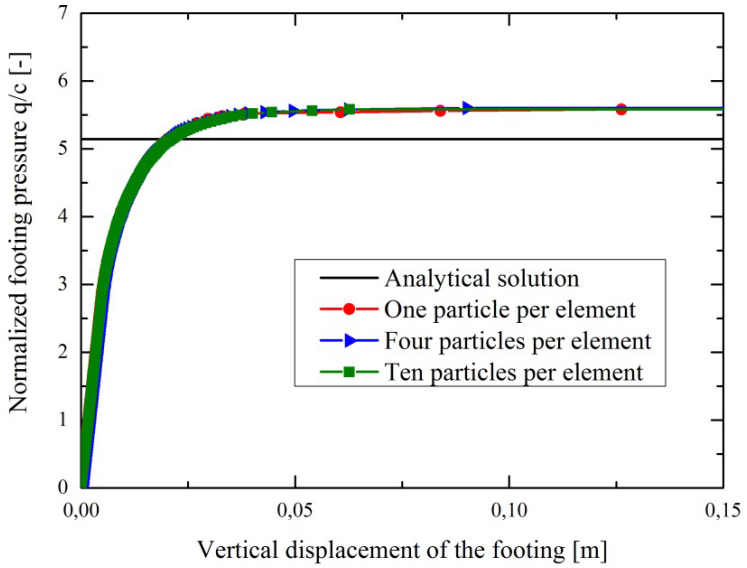

Figure 10: load displacement curve for the three different meshes zoomed on deformations between zero and 0.15 m

5 SUMMERY AND CONCLUSION

In this study the effect of different discretisations on the simulation results of a strip footing problem is investigated. After a short description of MPM working procedure and governing equations, the problem of strip footing with large deformation is analyzed using different meshes and different number of particles per element. Grid crossing of particles

which happen in the context of MPM influence the quality of the results. In the other side this particles moving to other elements enables MPM to simulate large deformations of the material. As shown in this study refining the mesh and increasing the initial number of particles per element helps to reduce this error.

REFERENCES

[1] Anderson, S. Anderson, L. Analysis of spatial interpolation in the material-point method *Computers and structures* (2010) **88**:506-518.

[2] Jassim, I.K. Hamad, F.M. and Vermeer, P.A. Dynamic material point method with applications in geomechanics. *Proc. 2nd Int. Symp. on Computational Geomechanics* (2011) Croatia.

[3] Hirt, C.W. Amsden, A.A. and Cook, J.L. An arbitrary Lagrangian-Eulerian computing method for all flow speeds. *J. Comput. Phys.* (1974) **14(3)**:227-253.

[4] Noh, W.F. CEL: A time-dependent, two-space-dimensional, coupled Eulerian-Lagrangian code. *Methods in Computational Physics* (1964) **3**:117-179.

[5] Belytschko, T. Lu, Y.Y. and Gu, L. Element-free Galerkin methods. *Int. J. Numer. Meth. Eng.* (1994) **37(2)**:229–256.

[6] Monaghan, J. J. An introduction to SPH. *Comput. Phys. Commun.* (1988) **48(1)**:89–96.

[7] Harlow, F.H. The particle-in-cell computing method for fluid dynamics. *Methods in Computational Physics* (1964) **3**:319–343.

[8] Brackbill, J.U. and Ruppel, H.M FLIP: A low dissipation particle-in-cell calculations of fluid flows in two dimensions. *J. Comput. Phys.*(1986) **65(2)**:314–343.

[9] Sulsky, D. Zhou, S.J. and Schreyer, H.L. Application of a particle-in-cell method to solid mechanics. *Comput. Phys. Commun.* (1995) **87**:236–252.

[10] Sulsky, D. and Schreyer, H.L. Axisymmetric form of the material point method with applications to upsetting and Taylor impact problems. *J. Comput. Method. Appl. M.* (1996) **139**:409–429.

[11] Bardenhagen, S.G. Brackbill, J.U. and Sulsky, D. The material-point method for granular materials. *Comput. Method. Appl. M.* (2000) **187**:529-541.

[12] Bardenhagen, S.G. and Kober, E.M. The generalized interpolation material point method. *Computer modelling in engineering and sciences* (2004) **5(6)**:477-496.

[13] Coetzee, C.J. Vermeer, P.A. and Basson, A.H. The modeling of anchors using the material point method. *Int. J. Numer. Anal. Met.* (2005) **29**:879-895.

[14] Burgess, D. Sulsky, D. & Brackbill, J.U. Mass matrix formulation of the FLIP particle-in-cell method. *J Comput Phys* (1992) **103** 1-15.

[15] Detournay, C. & Dzik, E. Nodal mixed discretization for tetrahedral elements, *4th International FLAC Symposium on Numerical Modeling in Geomechanics* (2006) Inc. Paper No. 02-07.

[16] Hill, R. *The mathematical theory of plasticity*. Clarendon press, Oxford (1950).